EMP Interaction Notes

Note III

Magnetic Field Shielding Degradation Due to Circular Apertures in Long Hollow Cylinders

21 September 1966

John N. Bombardt, Jr.
Electromagnetic Effects Branch
U. S. Army Engineer Research and Development Laboratories

Abstract

A series of experiments is described in which open-ended, long, circular cylinders with no apertures are considered. Experiments are described in which the same cylinders were employed with circular apertures introduced on the lateral surfaces. In each of the experiments a uniform axial magnetic field is applied externally. The experimental results are presented for both the non-aperture and aperture cases and in both cases, an attempt is made to correlate the experimental results with existing theory.

MAGNETIC FIELD SHIELDING DEGRADATION DUE TO CIRCULAR APERTURES IN LONG HOLLOW CYLINDERS

To investigate the effects of apertures on the shielding effectiveness of ideal, thin-walled, long circular cylinders, a series of experiments was performed in the ERDL Experimental Facility. This facility consists of essentially a solenoidal field generator which can expose small model test specimens to fairly uniform magnetic fields. Long cylinders are a particularly advantageous test specimen to deal with in this facility since instrumentation leads to sensors are shielded from the main solenoid field by the test specimen itself, and if the cylinders are long enough, cable pick-up from the main solenoid field is reduced to a minimum. Previous experiments and comparisons with theory [1] for the case of long circular cylinders that are integral shields with no apertures, immersed in uniform axial magnetic fields, have shown this to be the case. Thus, with the theory and experimental approach being fairly well understood for the case of transient responses of ideal circular cylinders, this case presented a logical starting point for more involved studies concerning degradation of shielding effectiveness due to apertures.

To begin, we will first consider measurements taken for an eight foot long copper cylinder with a diameter of 1/3 meter and a wall thickness of 0.014 inches. Before apertures were introduced, both axial and transverse measurements were made along the axis of this copper cylinder that was immersed in a uniform axial magnetic field. The axial solenoid field can be approximated by

---

[1] Superscripts refer to List of References at the end of this paper.

(1) $B_o(t) = A e^{-\alpha t} \sin \beta t$

where, for the measurements considered here,

$A = 2.07 \times 10^{-2}$

$\alpha = 2.09 \times 10^{5}$

$\beta = 0.73 \times 10^{5}$

which corresponds to a peak solenoid field of about 1.10×10^{-2} webers/m^2. Brown [2] has considered the transient response of thin-walled cylinders with no apertures for the external field given in equation (1).

The internal axial field, $B_i(t)$, derived by Brown for the thin-walled case with no apertures with the axial solenoid field given in equation (1) can be written in MKS units as

(2) $$B_i(t) = \frac{A\left(\frac{a}{b}\right)^{1/2}\omega_1}{\alpha^2 + (\beta - \omega_1)^2}\left\{\alpha e^{-\omega_1 t} - [\alpha \cos \alpha t + (\beta - \omega_1)\sin \alpha t] e^{-\beta t}\right\}$$

where

a = outer radius of cylinder

b = inner radius of cylinder

$$\omega_1 = \frac{2}{\mu \sigma b (a-b)}$$

Taking the material parameters μ and σ of the shield to be

$$\mu = \mu_o$$

and

$$\sigma = 5.56 \times 10^{7} \text{ mho/m},$$

all quantities in equation (2) are specified.

The comparison of the theoretical and experimental values of the internal axial magnetic induction field for early and late times is given in Figures 1 and 2. It should be mentioned that the measurements shown were taken on the axis of this copper cylinder at its geometrical center. The internal axial field, however, was found to be fairly uniform except near the open ends of the cylinder.

One last comment regarding the measurements for the copper cylinder with no apertures is that internal transverse measurements, measurements of any magnetic field that is transverse to the axis of the cylinder, were very low in magnitude and nearly below the range of instrumentation. For the case at hand with the external field that is present, we would not expect any transverse field components so that such null measurements would provide some measure as to the validity of the experiment.

Having obtained a good picture of what fields are present inside the above copper cylinder due to the shielding of the continuous solid wall, the next step was to investigate the effects of an aperture. A circular aperture was cut on the cylinder surface with a geodesic diameter of 3-3/8 inches. This is the same copper cylinder in which the previous results were obtained. Figure 3 illustrates the geometry employed for the measurements under consideration. Referring to this figure, measurements were made of the axial field B_y and of the transverse field B_z at points along the axis of the cylinder.

FIGURE 1. Comparison of Theoretical and Experimental Results
For a Hollow Copper Cylinder with no Apertures
(Early Time)

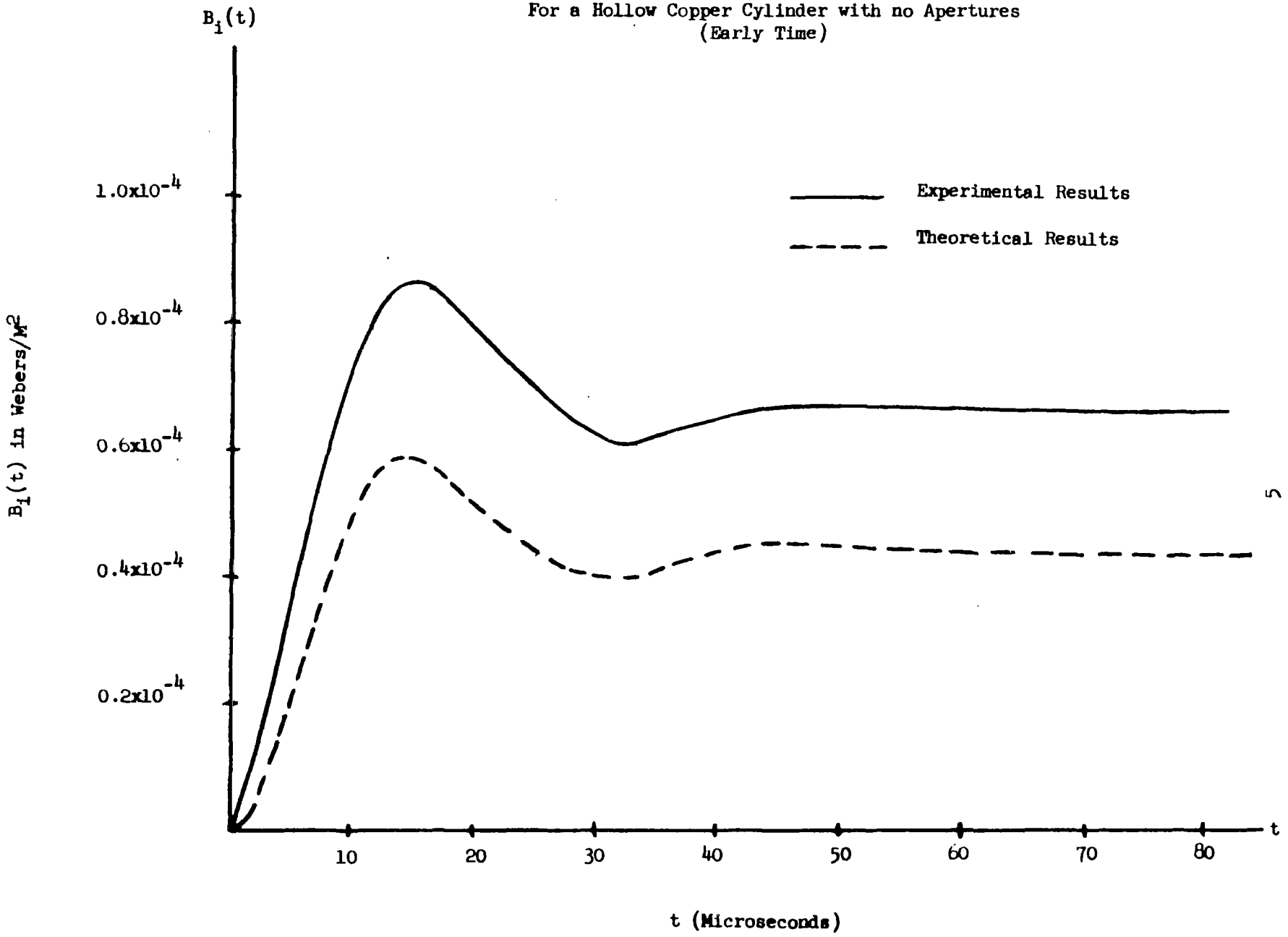

FIGURE 2. Comparison of Theoretical and Experimental Results
For a Hollow Copper Cylinder with no Apertures
(Late Time)

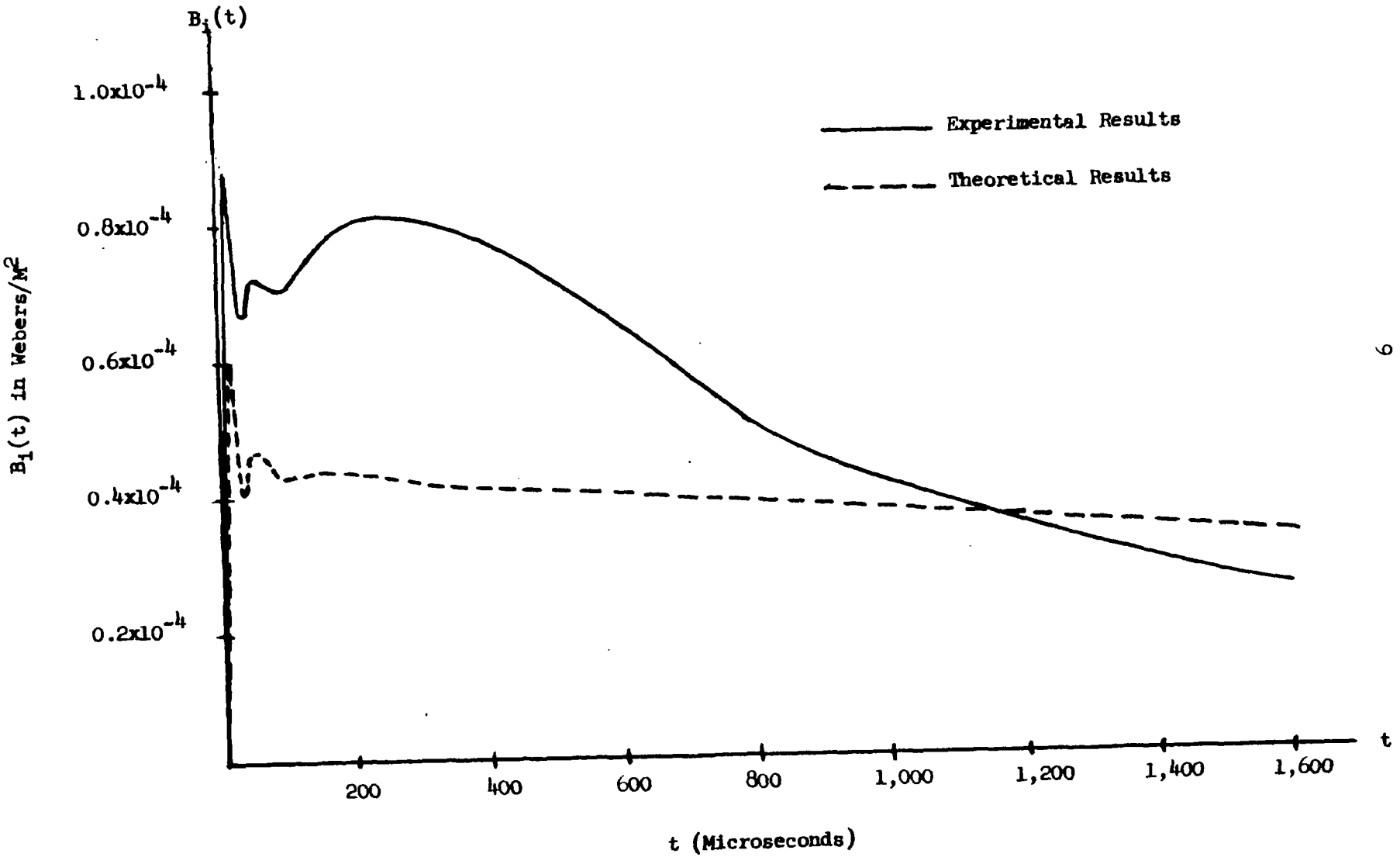

FIGURE 3. Geometry and Coordinates for the Analysis of Aperture Experiments

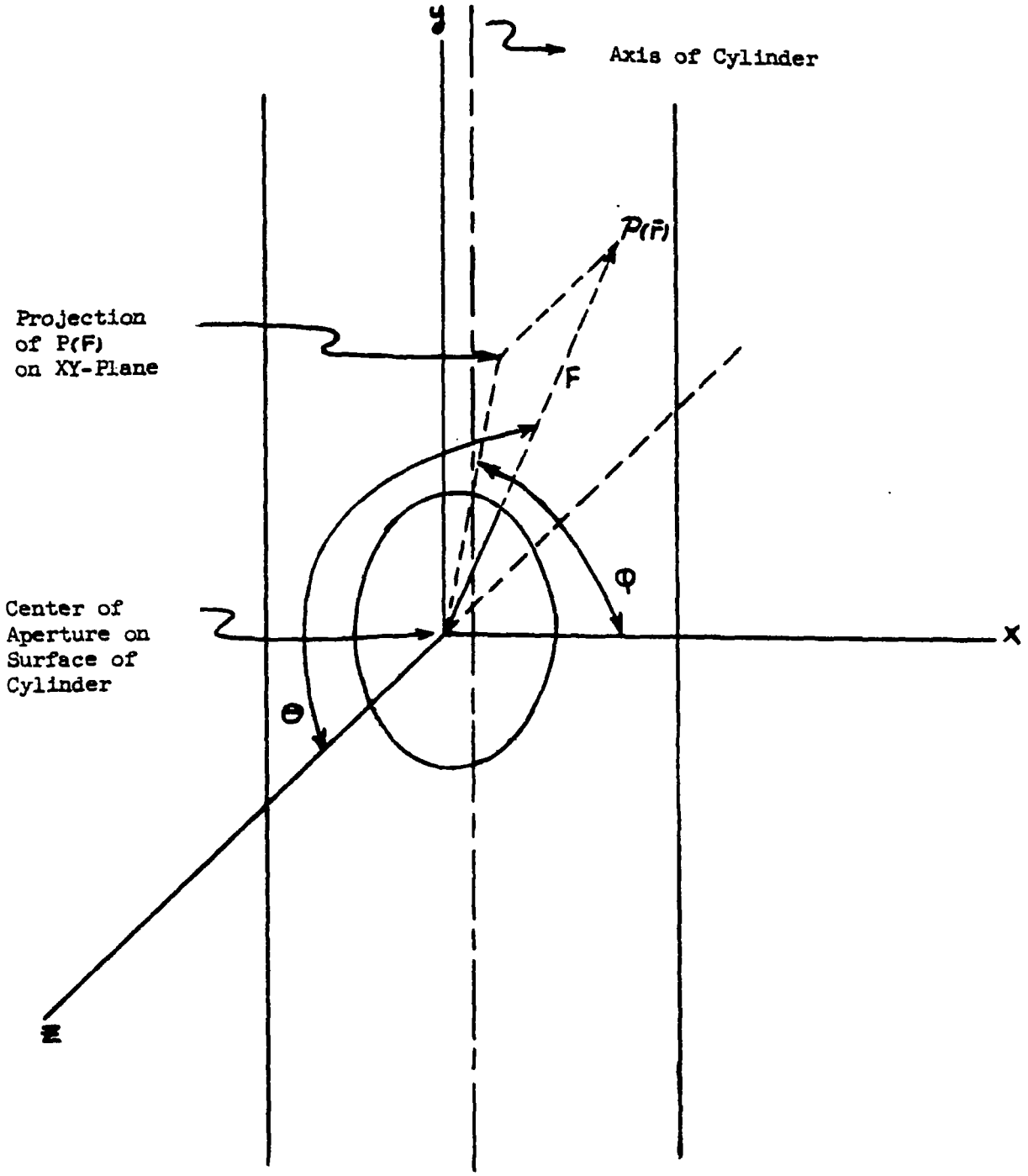

The results of the measurements for the axial field, B_y, showed that essentially the same B_y along the axis of the cylinder was present as that measured and calculated for the case of no aperture shown earlier. That is to say, no detectable or appreciable difference in the B_y field was observed at points along the axis of the cylinder. This does not exclude the existence of a B_y field due to the aperture that is much lower in magnitude than the B_y field for the case of no aperture.

The transverse field measurements, B_z, showed quite a different behavior for the aperture case than those similar null measurements for the solid wall cylinder with no aperture. The B_z field measurements for the aperture case exhibited temporal characteristics that quite closely matched those of the external axial field, B_o. In other words, the B_z time histories for the aperture case were damped sinusoids with cross-over and peak times very nearly the same as for the external axial field, B_o. The peak value scaling of this transverse field as a function of range from the center of the aperture for measurements taken along the axis of the cylinder will be shown after some other considerations.

In an attempt to understand the B_z field due to the aperture, it was felt that perhaps useful information could be obtained by applying Kaden's work.[3] Although Kaden does not solve our specific problem, he does consider the quasistatic case of a uniform magnetic field existing

over an infinite xy-plane that is very thin and infinitely conducting with a circular aperture of radius r_o. The aperture coordinates in Figure 3 have been chosen to coincide with those used by Kaden. One immediately questions the applicability of Kaden's work to our problem because of the difference in geometry and the quasistatic approximation. If nothing more than qualitative correlation is obtained, however, the exercise will have been useful in bolstering confidence in the experimental data.

Kaden obtains the following spherical field components in the region of interest $(\theta > \frac{\pi}{2})$:

$$(3) \qquad B_r = \frac{-4 r_o^3}{3\pi r^3} B_o \sin\varphi \sin\theta$$

$$(4) \qquad B_\varphi = \frac{2 r_o^3}{3\pi r^3} B_o \cos\varphi$$

and

$$(5) \qquad B_\theta = \frac{2 r_o^3}{3\pi r^3} B_o \sin\varphi \cos\theta$$

We have measured the B_z field component in our experiment with the copper cylinder with an aperture. Letting $\hat{k}$ denote a unit vector along the positive z-axis, the total B_z field component due to the aperture can be found from

$$(6) \qquad B_z = \bar{B} \cdot \hat{k}$$

where $\bar{B}$ and $\hat{k}$ are expressed in terms of spherical components. From geometrical considerations, it is easily found that

(7) $\hat{k} = \hat{r}\cos\theta - \hat{\theta}\sin\theta$ (see appendix)

where $\hat{r}$ and $\hat{\theta}$ are unit vectors in the directions of r and θ, respectively. Using equations (6) and (7) we have then simply,

(8) $B_z = B_r \cos\theta - B_\theta \sin\theta$.

With expressions (3), (5), and (8) we obtain the desired B_z component in terms of r, θ, and φ,

(9) $B_z = \frac{-2r_0^3}{\pi r^3} B_0 \sin\varphi \sin\theta \cos\theta$.

A result of the quasistatic approximation is that the field components in the region of interest will possess the same temporal characteristics as the external field. This is encouraging in that this is precisely what was observed in the cylinder with an aperture experiment for the B_z field component. Thus both theoretically and experimentally, it is found that the temporal characteristics of the aperture fields should resemble those of the external field for the case at hand.

The following table gives the position coordinates and the corresponding B_z^{peak} values obtained from Kaden's theory:

r (meters)	θ	φ	B_z^{peak} (webers/M^2)
1.67×10^{-1}	180°	-90°	0
1.69×10^{-1}	171°	-90°	0.183×10^{-4}
1.75×10^{-1}	163°	-90°	0.288×10^{-4}
1.84×10^{-1}	155°	-90°	0.336×10^{-4}
1.95×10^{-1}	148°	-90°	0.333×10^{-4}
2.10×10^{-1}	143°	-90°	0.285×10^{-4}
2.44×10^{-1}	135°	-90°	0.189×10^{-4}
3.04×10^{-1}	123°	-90°	0.085×10^{-4}
4.15×10^{-1}	110°	-90°	0.022×10^{-4}

The above results along with the experimental results are plotted in Figure 4. In passing, it should be noted that the zero field value occurs directly below the center of the aperture on the axis of the cylinder so that the corresponding range is just the radius of the cylinder. Furthermore, the maximum field value occurs roughly below the edge of the aperture on the axis of the cylinder. Both of these observations are found theoretically and experimentally as can be seen in Figure 4. Lastly, it was found experimentally that there was a change in polarity of B_z as the measurement point moved from $\varphi = -90^\circ$ along the axis of the cylinder to $\varphi = +90^\circ$ along the axis of the cylinder, and more generally, the measurements exhibited odd symmetry in φ along the axis of the cylinder. This can be seen also in expression (9).

FIGURE 4. Comparison of Theoretical and Experimental Peak Field Values for the Aperture Problem

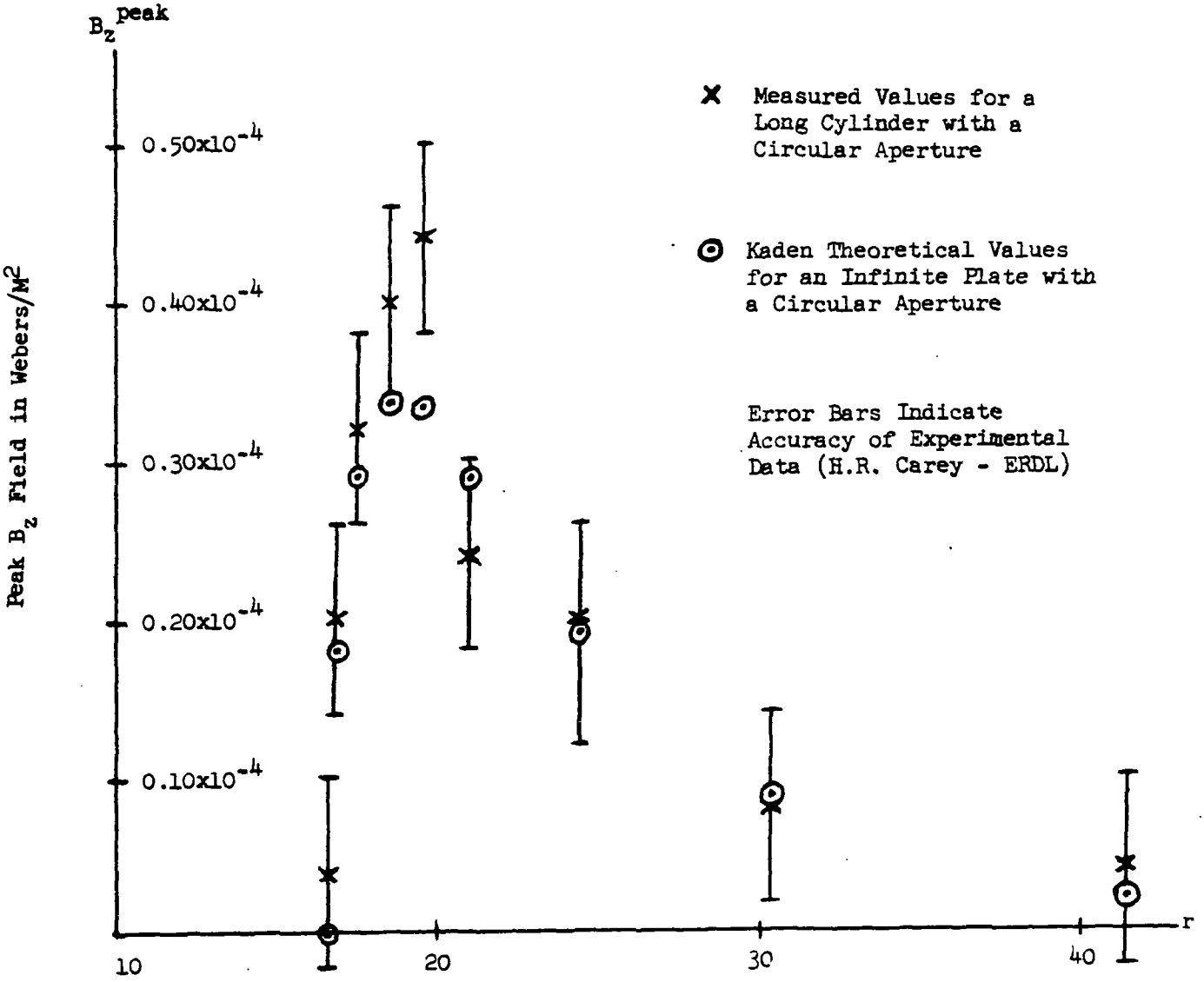

To obtain an idea as to the effect of the thickness of the shield when apertures are present, another experiment was performed. The same diameter shield, 1/3 meter, this time made of aluminum of thickness nominally 3/16 inch was employed and an aperture with the same geodesic diameter of 3-3/8 inches was cut in the same position as for the copper cylinder. The same measurements were made on this aluminum cylinder with an aperture that were made on the copper cylinder with an aperture. The measurements made on the aluminum cylinder actually served a dual purpose; the data taken would serve to help answer the above mentioned thickness question in relation to apertures and also provide the opportunity to observe aperture fields alone since diffusion fields would be very low in comparison to expected aperture fields. The results for the transverse field, B_z, in the aluminum cylinder were essentially the same as those obtained for the copper cylinder that were discussed earlier and plotted in Figure 4. Furthermore, the results of the aluminum cylinder showed that the axial field, B_y, was much lower in magnitude than the B_z component.

Consider now, the axial field, B_y, due to the aperture in either the aluminum or copper cylinder experiment. The total B_y field component due to the aperture can be found from

$$B_y = \bar{B} \cdot \hat{j} \tag{10}$$

where $\hat{j}$ is a unit vector along the positive y-axis and both $\hat{j}$ and $\bar{B}$ are expressed in terms of spherical components. From geometrical considerations, it can be found that

(11) $\hat{j} = \hat{r}\sin\theta\sin\varphi + \hat{\theta}\cos\theta\sin\varphi + \hat{\varphi}\cos\varphi$ (See Appendix)

where $\hat{r}$, $\hat{\theta}$, and $\hat{\varphi}$ are unit vectors for the respective spherical coordinates. The total B_y field component can be then expressed as

(12) $$B_y = B_r \sin\theta\sin\varphi + B_\theta \cos\theta\sin\varphi + B_\varphi \cos\varphi .$$

Substituting (3), (4), and (5) into (12), we have

$$B_y = \frac{2r_0^3}{3\pi r^3} B_0 (-2\sin^2\theta\sin^2\varphi + \sin^2\varphi\cos^2\theta + \cos^2\varphi)$$

or

$$B_y = \frac{2r_0^3}{3\pi r^3} B_0 [\sin^2\varphi(\cos^2\theta - 2\sin^2\theta) + \cos^2\varphi],$$

so that we obtain

(13) $$B_y = \frac{2r_0^3}{3\pi r^3} B_0 (1 - 3\sin^2\theta\sin^2\varphi).$$

To estimate the relative magnitude of B_y with respect to B_z, we form their quotient at $\varphi = -\pi/2$ so that along the axes of our cylinders we would expect

(14) $$\left|\frac{B_y}{B_z}\right|_{\varphi=-\pi/2} = \frac{1}{3}\left|\frac{1 - 3\sin^2\theta}{\sin\theta\cos\theta}\right|_{\varphi=-\pi/2}.$$

At the measurement point of maximum B_z, namely $\theta = 155^\circ$, we find

$$\left| \frac{B_y}{B_z} \right|_{\varphi=-\pi/2,\theta=155^\circ} \approx 0.4$$

Here again the Kaden theory yields some verification of the experimental data.

In conclusion, it might be well to emphasize the restrictions imposed in any application of Kaden's aperture theory. The quasistatic approximation appears to be quite good for frequencies below a megacycle when dealing with small idealized enclosures. However, for both higher frequencies and large non-ideal structures, the validity of the quasistatic approximations must be questioned. The effect of higher frequencies for the case of small idealized structures with apertures can probably be investigated experimentally. The problem of life-size structures with apertures for the full frequency range of interest should be considered in analytical detail to determine what approximations can be made and to what extent they are valid.

I would like to thank and acknowledge Mr. A. R. Bemis, Mr. H. R. Carey, and Mr. R. Prochazka for the engineering support and the measurements taken in the above considered experiments.

APPENDIX

Consider the following diagram with the indicated unit vectors:

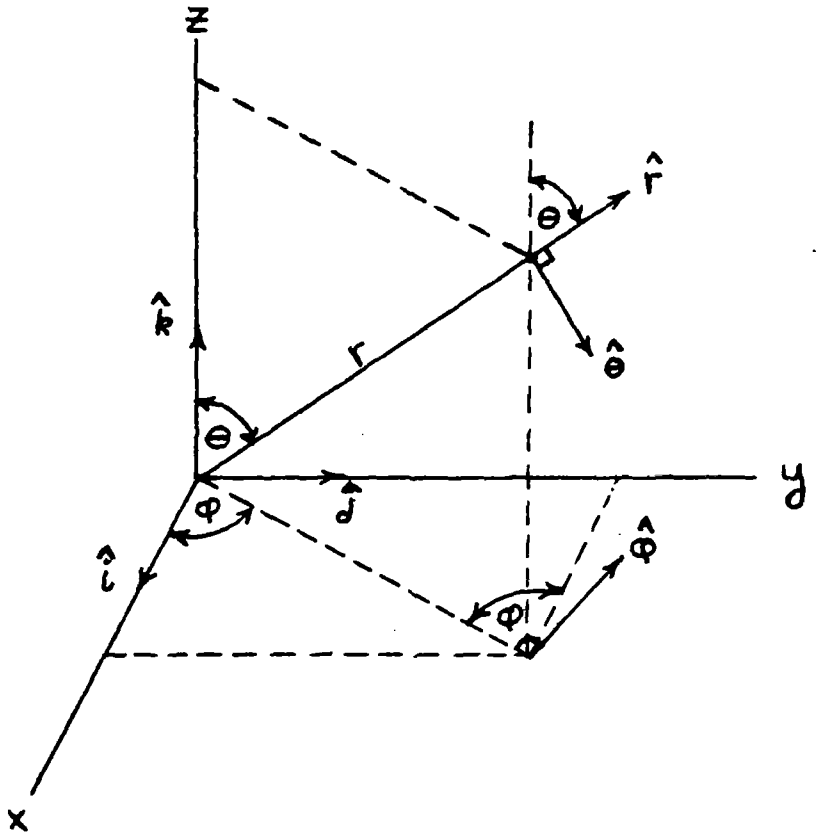

From the diagram, the unit vector $\hat{k}$ can be expressed as,

$$\hat{k} = \hat{r}\cos\theta - \hat{\theta}\cos(\pi - \pi/2 - \theta)$$

so that

$$\hat{k} = \hat{r}\cos\theta - \hat{\theta}\sin\theta. \qquad \text{(A-1)}$$

Similarly, the unit vector $\hat{j}$ can be expressed as,

$$\hat{j} = \hat{r}\sin\theta\sin\varphi + \hat{\theta}\sin(\pi - \pi/2 - \theta)\sin\varphi + \hat{\varphi}\sin(\pi/2 - \varphi)$$

so that

$$\text{(A-2)} \quad \hat{j} = \hat{r}\sin\theta\sin\phi + \hat{\theta}\cos\theta\sin\phi + \hat{\phi}\cos\phi.$$

Finally, the unit vector $\hat{i}$ can be expressed as,

$$\hat{i} = \hat{r}\sin\theta\cos\phi + \hat{\theta}\sin(\pi - \pi/2 - \theta)\cos\phi - \hat{\phi}\cos(\pi/2 - \phi)$$

so that

$$\text{(A-3)} \quad \hat{i} = \hat{r}\sin\theta\cos\phi + \hat{\theta}\cos\theta\cos\phi - \hat{\phi}\sin\phi.$$

LIST OF REFERENCES

1. D. B. Dinger, J. N. Bombardt, W. J. Haas, Final Technical Report on Nuclear Electromagnetic Pulse Effects Research and Development Studies in Support of the Nike-X Electrical Power System Program (U), USAERDL Report, 5 November 1965.(SECRET-RD)

2. R. N. Ghose, G. L. Brown, EMP Energy Coupling Studies (U), American Nucleonics Corporation, Final Report under Contract DA-49-146-XZ-445, 14 January 1966. Official Use Only (DASA - 1753)

3. Heinrich Kaden, Wirbelstrome und Schirmung in der Nachrichtentechnik, Technische Physik in Einzeldarstellungen 10, Springer-Verlag, 1959.